JOURNAL OF APPLIED POLYMER SCIENCE VOL. 19, PP. 2033–2058 (1975)

Strain Energy Functions of Rubber. I. Characterization of Gum Vulcanizates

A. G. JAMES, A. GREEN, and G. M. SIMPSON, *Dunlop Research Center, Kingsbury Road, Erdington, Birmingham, England*

Synopsis

A plot of principal stress difference versus principal extension ratios has been used as a graphic representation of general deformation. Two analytic forms of the strain energy function for isotropic, incompressible materials are suggested. These involve five or nine terms, the coefficients of which are found by regression to the general deformation plot. The resulting stress–strain equations are used to predict particular deformations, for example, simple extension, and are also evaluated in model engineering design experiments. These experiments use iterative techniques to predict the shapes and pressures of inflated diaphragms and tubes, and it is shown that the equations lead to accurate results even at relatively high extensions.

INTRODUCTION

In rubber engineering, computer-oriented iterative techniques and methods have led to the possibility of solving more complex design problems. The accuracy of these techniques depends, however, on the accuracy to which the elastic nature of the design material can be defined, that is, on the accurate knowledge of the strain energy function of the deformation of the material or the stress–strain equations which are derived from it.

There are two main approaches in defining constitutive equations to describe the elastic nature of rubber-like materials. The molecular approach considers the response of the molecular network to deformation. Typically, there is the Gaussian theory where elasticity parameters are calculated from such quantities as finite molecular length and molecular weight between crosslinks. There is also the phenomenological approach where elasticity theory is modified often intuitively and a postulated form is fitted to experimental results by regression.

Because of the high extensibility of these materials and because of nonlinear force–deformation relationships up to these high extensions, a dilemma is encountered when trying to define a strain energy function or stress–strain equation. The particular constitutive equation will contain one or more constants which must be determined, and the dilemma arises when the investigator is forced to choose a particular type of deformation under which the constants are to be calculated.

Many forms of strain energy function have been postulated with constants which adjust to fit the shape of the stress–strain curve in, say, simple extension.

Some of these will be described later. All this procedure proves is that regression techniques work. If the regression had been performed to data in pure shear, an equally good fit would have been obtained with an entirely different set of "material" constants.

To overcome this, many investigators have included experimental data from more than one type of deformation in their regression analysis, in order that their postulated form of strain energy function may be shown to be as general as possible. Rivlin and Saunders[1] included simple extension and uniaxial compression on the same diagram. Other authors have looked at combined tension and extension, inflation and torsion, and so on.

However, as Treloar points out,[2] the process of modifying or correcting a strain energy function to suit a set of data is nothing more than the "three-dimensional analogue of simple curve fitting." Thus, until a generalized molecular hypothesis is found, any phenomenologic strain energy function that is postulated is merely a convenient mathematical representation, and no meaning should be attached to the numerical constants over and above that of simpler regression coefficients.

Having recognized this fact, the problem of finding stress–strain equations or strain energy functions for a particular material is simplified to finding an experimental method which involves general deformation and a regression equation which contains enough terms to fit accurately to the results of this experiment. The test of a particular form is, then, the success with which it can be applied to practical situations.

This paper goes on to describe such an experimental method and suggests a graphic form for presentation of the results. Many of the strain energy functions which have been proposed in the literature are judged against this criteria. Finally, functions are suggested which have proved to be accurate in a number of practical tests.

GENERAL HOMOGENEOUS STRAIN

Elasticity Theory

When a body is deformed, the elastic strain energy W may be expressed in terms of the strain invariants I_1, I_2, and I_3:

$$W = \sum_{ijk=0}^{\infty} C_{ijk}(I_1 - 3)^i(I_2 - 3)^j(I_3 - 1)^k \cdots \tag{1}$$

where I_1, I_2, and I_3 are defined as the trace, cofactor trace, and determinant of the covariant strain tensor γ, where

$$\gamma = \begin{vmatrix} \lambda_i^2 & 0 & 0 \\ 0 & \lambda_j^2 & 0 \\ 0 & 0 & \lambda_k^2 \end{vmatrix}$$

and λ_i λ_j, and λ_k are the principal extension ratios; C_{ijk} are constants. Thus,

$$\begin{aligned} I_1 &= \mathrm{Tr}(\gamma) = \lambda_i^2 + \lambda_j^2 + \lambda_k^2 \\ I_2 &= \mathrm{Tr}(\mathrm{co}\gamma) = \lambda_i^2\lambda_j^2 + \lambda_j^2\lambda_k^2 + \lambda_k^2\lambda_i^2 \cdots \\ I_3 &= \mathrm{Det.}\ \gamma = \lambda_i^2\lambda_j^2\lambda_k^2 \end{aligned} \tag{2}$$

The principal true stress σ for pure homogeneous deformation of an isotropic elastic material is obtained form W:

$$\sigma_i = \left| \frac{1}{\lambda_j \lambda_k} \right| \times \frac{\partial W}{\partial \lambda_i} \cdots \tag{3}$$

From eqs. (1), (2), and (3), it can be shown that the difference between two orthogonal stresses takes the form

$$\sigma_i - \sigma_j = 2/\sqrt{I_3}\,(\lambda_i^2 - \lambda_j^2) \left| \frac{\partial W}{\partial I_1} + \lambda_k^2 \frac{\partial W}{\partial I_2} \right| \cdots \tag{4}$$

where for incompressible materials $I_3 = 1.0$.

Pure Homogeneous Strain

For general homogeneous strain, the three principal extension ratios λ_1, λ_2, and λ_3 may take any value consistant with the incompressibility condition

$$\lambda_1 \lambda_2 \lambda_3 = 1.$$

Thus, if any two are considered as independent variables, the third is necessarily determined. Treloar[4] and Rivlin and Saunders[1] described apparatus and experiments to achieve just such independent variation of two of the three principal orthogonal extension ratios; and recently these ideas were put on a sound engineering basis by Kawai et al.[5] A similar apparatus has been constructed and is in use in Dunlop Ltd., Central Research and Development Division.

EXPERIMENTAL

Photographs of the apparatus and a test piece extended to $\lambda = 3.5$ in two directions are given in Figure 1. The apparatus is designed to impart independently controlled strains to a square test piece such that the two maximum

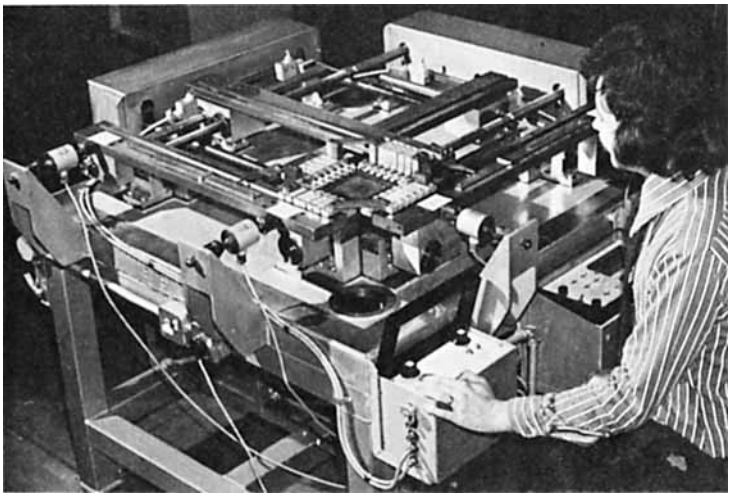

(a)

Fig. 1 (*continued*)

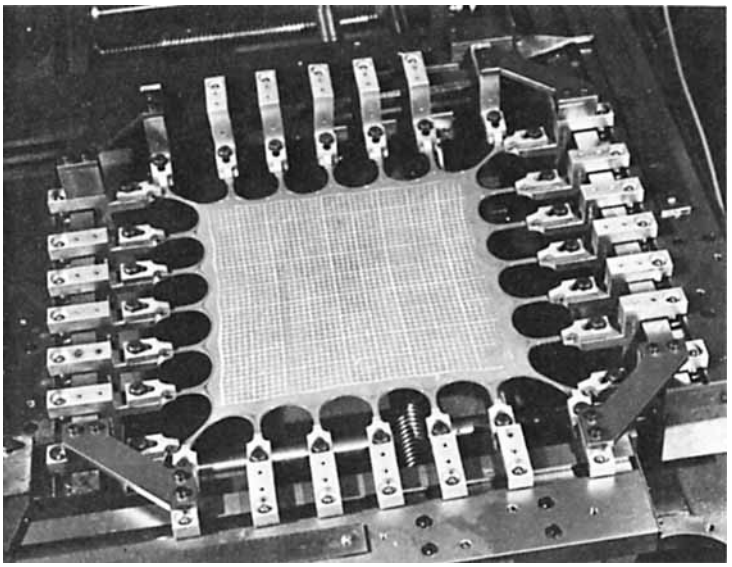

(b)

Fig. 1. (a) General view of biaxial tensile test apparatus. (b) Close-up of test piece extended to $\lambda = 3.5$ in two directions.

stresses are at right angles. This is achieved by having two moving cross heads incorporating sliding clamps which grip the specially designed test piece at seven points along each side. The clamps are mounted on roller bearings so that they can move freely along the cross heads and can therefore accommodate the deformation of the orthogonal direction. The points at which the test piece is gripped are much thicker than the test area, so that as the test piece is extended, the strain occurs in the test area rather than at the clamps. However, the thicker edges are "scalloped" to within 1 mm of the test piece edge such that their effective contribution to the total cross section is less than 5%. A lithographic plate is used to draw a grid of 2 cm^2 (subdivided into 2-mm squares) on the test piece to facilitate strain measurement. In Figure 1, the regularity of the grid is an indication of the homogeneity of the strain.

The moving cross heads slide on linear bearings and are moved by lead screws driven by motors through chain drives. The loads are measured by paired load cells connected by universal joints to the "fixed" cross heads. The electrical output from each pair of load cells is fed to a digital meter which displays individual output or the sum of the outputs of the paired load cells. At present, a thermal chamber incorporating a remote strain measurement technique is under construction.

Thus, two principal extension ratios, λ_1 and λ_2, can be selected independently up to a maximum of 3.5 in each direction on the standard test piece (10 cm $\times$ 10 cm).

The general homogeneous strain experiment yields values of the applied orthogonal engineering stresses f_1, f_2 at extensions λ_1, λ_2. It is also known that f_3, the stress in the thickness direction, is zero and $\lambda_3 = 1/\lambda_1\lambda_2$ in an incompressible material.

TABLE I
Natural Rubber Vulcanizate—Compounding Details[a]

Ingredient	Parts per hundred of polymer
Natural rubber	100.00
Sulfur	2.50
CBS	0.50
Stearic acid	2.00
Zinc oxide	5.00
Mineral oil	5.00
Nonox ZA	0.15
Ble 25	0.85

[a] The vulcanizate was cured for 50 min at 135°C.

The principal true stresses are calculated remembering that

$$\sigma_i = f_i\lambda_i.$$

The experimental results should satisfy eq. (4), although the choice of axes is entirely arbitrary and σ_i and σ_j may be taken to be σ_1, σ_2, or σ_3.

RESULTS

A sulfur-cured natural-rubber test piece was used in the general homogeneous strain experiment; the compounding details and conditions of vulcanization are given in Table I. The test piece was stress softened by stretching it ten times to the maximum deformation, and then forces were measured at a number of fixed values of λ_1 in the range $\lambda_2 = 1\sqrt{\lambda_1} \rightarrow \lambda_1$. The test piece was allowed approximately 5 min to relax to a quasi-equilibrium state at each measurement. The strain in the thickness direction was calculated from the incompressibility condition. Forces were converted to engineering stresses and then true stresses. Allowance was made for the small effect of the clamping edge on the cross-sectional area.

In Figure 2, the experimental measurements are presented as suggested by Kawai et al.,[6] that is, σ_1, σ_2 is plotted as a function of λ_2 for constant values of λ_1. The (○) symbols in Figure 2 represent data plotted such that the arbitrary choice $\sigma_i = \sigma_1$, $\sigma_j = \sigma_2$ is made and the (×) symbols represent data plotted such that $\sigma_i = \sigma_1$, $\sigma_j = \sigma_3 = 0$. This plot was taken as a criterion of general homogeneous strain, and many of the suggested forms for general stress–strain equations have been weighed against this criterion. The experimental data are tabulated in Table II.

Choosing a Regression Equation

The purpose of the work described in this paper was to decide upon an analytic form of stress–strain equation suitable for use in design calculations. However, W has been expressed as an infinite series and eqs. (4) are only useful if an empirical form for $\partial W/\partial I_1$ and $\partial W/\partial I_2$ can be found. A number of forms suggested in the literature have been examined. These equations were examined against the results of the general homogeneous strain experiments and against criteria which have been used by other workers; for example, the stress–strain

TABLE II
PHS Plot Experimental Data Natural-Rubber Gum

Extension ratio λ_1	Extension ratio λ_2	Engineering stress F_1/A_0, MN/m²	Engineering stress F_2/A_0, MN/m²
1.3	0.93	0.366	0.084
1.3	1.0	0.422	0.235
1.3	1.1	0.450	0.338
1.3	1.2	0.497	0.431
1.3	1.3	0.525	0.516
1.5	0.95	0.563	0.216
1.5	1.0	0.572	0.300
1.5	1.1	0.600	0.413
1.5	1.2	0.628	0.507
1.5	1.3	0.647	0.572
1.5	1.4	0.675	0.638
1.5	1.5	0.685	0.685
1.7	0.95	0.666	0.281
1.7	1.0	0.685	0.356
1.7	1.1	0.722	0.469
1.7	1.2	0.741	0.553
1.7	1.3	0.760	0.610
1.7	1.4	0.769	0.666
1.7	1.5	0.788	0.732
1.7	1.6	0.807	0.769
1.7	1.7	0.816	0.816
2.0	0.93	0.825	0.338
2.0	1.0	0.844	0.441
2.0	1.1	0.863	0.525
2.0	1.2	0.882	0.591
2.0	1.3	0.900	0.657
2.0	1.4	0.919	0.713
2.0	1.5	0.928	0.760
2.0	1.6	0.947	0.807
2.0	1.7	0.957	0.854
2.0	1.8	0.966	0.900
2.0	1.9	0.985	0.938
2.0	2.0	0.994	0.985
2.5	0.91	1.032	0.441
2.5	1.0	1.041	0.553
2.5	1.1	1.051	0.619
2.5	1.2	1.088	0.694
2.5	1.3	1.097	0.741
2.5	1.4	1.107	0.797
2.5	1.5	1.126	0.844
2.5	1.6	1.144	0.891
2.5	1.7	1.154	0.928
2.5	1.8	1.163	0.976
2.5	1.9	1.173	1.013
2.5	2.0	1.191	1.069
2.5	2.1	1.210	1.107
2.5	2.2	1.238	1.154
2.5	2.3	1.257	1.219
2.5	2.4	1.266	1.257
2.5	2.5	1.276	1.294
3.0	0.86	1.304	0.488

(*continued*)

TABLE II (*continued*)

Extension ratio λ_1	Extension ratio λ_2	Engineering stress F_1/A_0, MN/m²	Engineering stress F_2/A_0, MN/m²
3.0	1.0	1.313	0.638
3.0	1.2	1.345	0.769
3.0	1.4	1.360	0.872
3.0	1.6	1.388	0.957
3.0	1.8	1.426	1.060
3.0	2.0	1.463	1.154
3.0	2.2	1.491	1.248
3.0	2.4	1.510	1.341
3.0	2.6	1.557	1.444
3.0	2.8	1.604	1.557
3.0	3.0	1.651	1.670
3.5	0.84	1.548	0.544
3.5	1.0	1.576	0.722
3.5	1.2	1.613	0.872
3.5	1.4	1.642	0.985
3.5	1.6	1.679	1.079
3.5	1.8	1.717	1.182
3.5	2.0	1.745	1.276
3.5	2.2	1.763	1.369
3.5	2.4	1.801	1.473
3.5	2.6	1.848	1.576
3.5	2.8	1.895	1.707
3.5	3.0	1.970	1.838
3.5	3.2	2.064	1.998
3.5	3.4	2.139	2.186

curves in simple extension, pure shear, and equibiaxial extension and the Mooney-Rivlin plot $[f/(\partial W/\partial I_1 + 1/\lambda\ \partial W/\partial I_2)]$ versus $1/\lambda$ for tension and compression. As a further constrain on the acceptability of any particular form, model design experiments have been considered in which rubber is deformed in a general and complex way. These experiments involve the prediction of shapes, sizes, and pressures of diaphragms and tubes which were inflated to fixed surface strains.

It was possible to eliminate many of the suggested forms by considering the results of Kawai et al.[6] for general homogeneous strain where $\partial W/\partial I_1$ was shown to depend on I_1 and I_2. Many of the suggested forms[7-11] show $\partial W/\partial I_1$ or $\partial W/\partial I_2$ or both to be independent of either or both of the strain invariants. As the present investigation confirmed the results of Kawai, these forms were eliminated from this investigation.

Another type of approach to this problem has been suggested by Valanis and Landel[12] and Ogden,[13] where the strain energy function was redefined in terms of strains or extension ratios rather than in terms of strain invariants. Kawai et al.[6] criticized the Valanis-Landel hypothesis for the use of the empirical relation

$$W'(\lambda) = 2\mu \ln \lambda$$

in that it did not adequately represent the strip biaxial data of Kawai. This empirical substitution also leads to a stress–strain equation involving only one material constant. In this investigation, it was found that to predict both size

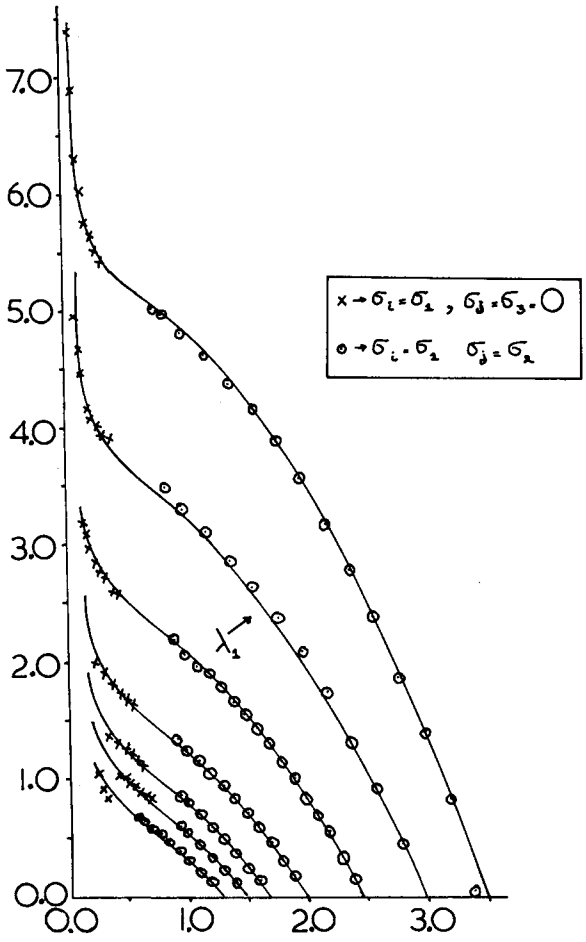

Fig. 2. Pure homogeneous strain plot (PHS plot) for NR gum. The regression lines are calculated using the third-order invariant approximation of the strain energy function. Abscissa: extension ratio λ_2; ordinate: stress $\sigma_i - \sigma_j$ (MN/m^2).

and shape in our model inflation experiments it was necessary to have stress–strain equations containing at least two material constants. However, the condition of separability of strains resulting in stress difference equations of the form

$$\sigma_{11} - \sigma_{22} = \lambda_1 W'(\lambda_1) - \lambda_2 W'(\lambda_2)$$

would suggest that the lines on the graph Figure 2 should be independent of λ_1. By shifting these lines vertically, this is seen to be true for this material over the range of deformation examined, and this also applies to the form suggested by Ogden. A study of the transposition of these lines may lead to a more useful empirical form of the Valanis-Landel hypothesis.

So far, none of these suggested modifications of elasticity theory has proved sufficiently general for our purposes. A more rewarding approach was suggested by Tschoegl[14] and Bidemann,[15] this involved strict adherence to elasticity theory, and more accurate approximation to the quantities $\partial W/\partial I_1$ and $\partial W/\partial I_2$ being obtained by including higher order terms from the expansion of the strain energy function.

Approximating the Strain Energy Function

For incompressible materials ($I_3 = 1.0$), the strain energy function eq. (1) takes the form

$$W = \sum_{ij=0}^{\infty} C_{ij} (I_1 - 3)^i (I_2 - 3)^j \cdots \tag{5}$$

This expands as follows:

$$W = C_{10}(I_1 - 3) + C_{01}(I_2 - 3) + C_{11}(I_1 - 3)(I_2 - 3) + C_{20}(I_1 - 3)^2 + C_{02}(I_2 - 3)^2 \cdots \text{ etc.}$$

(Note: The term C_{00} is always taken to be zero.)

This series may be truncated according to either of the following conventions:

(a) *Orders of Invariants*

First Order (Including only First-Order Terms in $(I_1 - 3)$ and $(I_2 - 3)$)

$$W = C_{10}(I_1 - 3) + C_{01}(I_2 - 3)$$

$$\therefore \frac{\partial W}{\partial I_1} = C_{10} \quad \text{and} \quad \frac{\partial W}{\partial I_2} = C_{01}.$$

This results in the Mooney stress–strain equation.

Second Order (Including up to Second-Order Terms in $(I_1 - 3)$ and $(I_2 - 3)$)

$$W = C_{10}(I_1 - 3) + C_{01}(I_2 - 3) + C_{11}(I_1 - 3)(I_2 - 3) + C_{20}(I_1 - 3)^2 + C_{02}(I_2 - 3)^2.$$

Third Order (Including up to Third-Order Terms in $(I_1 - 3)$ and $(I_2 - 3)$

$$W = C_{10}(I_1 - 3) + C_{01}(I_2 - 3) + C_{11}(I_1 - 3)(I_2 - 3) + C_{20}(I_1 - 3)^2 + C_{02}(I_2 - 3)^2 + C_{21}(I_1 - 3)^2(I_2 - 3) + C_{12}(I_1 - 3)(I_2 - 3)^2 + C_{30}(I_1 - 3)^3 + C_{03}(I - 3)^3$$

(b) *Order of Deformation*

It is also possible to choose terms out of the expansion of W such that only certain orders of deformation (i.e., powers of λ) are included. Sato[16] has truncated the series by taking terms which include (a) only squares of the extension ratios, (b) squares and fourth powers, (c) squares, fourth, and sixth powers, and so on. If eq. (5) is expanded in this way, which will be called the deformation approximation, then the first-, second-, third-, and fourth-order approximations are as follows:

First Order

$$W = C_{10}(I_1 - 3).$$

This leads to the simple Gaussian stress–strain equation

$$\sigma_1 - \sigma_2 = C_{10}(\lambda_1^2 - \lambda_2^2).$$

Second Order. The terms contained in the expansion of W are

1st order	$C_{10}(I_1 - 3)$
2nd order	$C_{20}(I_1' - 3)^2$
	$C_{01}(I_2 - 3)$

Third Order. The terms contained in the expansion of W are

1st order	$C_{10}(I_1 - 3)$
2nd order	$C_{20}(I_1 - 3)^2$
	$C_{01}(I_2 - 3)$
3rd order	$C_{30}(I_1 - 3)^3$
	$C_{11}(I_1 - 3)(I_2 - 3)$

Fourth Order. The terms contained in the expansion of W are

1st order	$C_{10}(I_1 - 3)$
2nd order	$C_{20}(I_1 - 3)^2$
	$C_{01}(I_2 - 3)$
3rd order	$C_{30}(I_1 - 3)^3$
	$C_{11}(I_1 - 3)(I_2 - 3)$
4th order	$C_{40}(I_1 - 3)^4$
	$C_{21}(I_1 - 3)^2(I_2 - 3)$
	$C_{02}(I_2 - 3)^2$

There are certain observations which can be made about this method of approximation referred to in future as deformation approximation. First-order deformation approximation results in the Gaussian form, whereas invariant approximation does not. Conversely, the Mooney equation is not a logical approximation in terms of deformations.

Comparing the Different Approximations

In order to possess generality, the constants in a particular form of strain energy function or stress–strain equation must represent experimental data involving pure homogeneous strain, and the greater the range of these data, the better. In the section on general homogeneous strain, an experiment to obtain such data was described. Figure 2 is a graphic representation of these data (PHS plot-pure homogeneous strain) obtained over as large a range as was practically possible. The solid lines in Figure 2 are regression lines which were calculated from stress–strain equations derived from an expansion of

$$W = \sum_{ij=0}^{\infty} C_{ij}(I_1 - 3)^i (I_2 - 3)^j$$

as far as terms of the third order in the invariants. This involves nine constants C_{ij}.

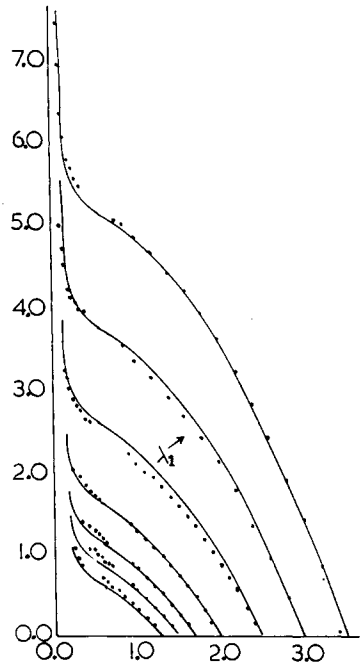

Fig. 3. PHS plot for NR gum using Mooney function. Abscissa: extension ratio λ_2; ordinate: stress $\sigma_i - \sigma_j$ (MN/m²).

It can be shown that other forms of expansion of W will predict the form of the PHS plot with varying degrees of accuracy; for example, the so-called Mooney equation,

$$\sigma_1 - \sigma_2 = 2(\lambda_1^2 - \lambda_2^2)\left|C_{10} + \lambda_3^2 C_{01}\right|$$

which involves only the two constants C_{10} and C_{01}.

In Figure 3, it is shown that the general shape of the PHS plot is predicted by this equation, although the correspondence of the regression lines and the experimental data is not as good as in Figure 2. If the overall range of deformation is reduced, the fit is better. It can also be shown that the Mooney equation which fits these data will successfully predict such things as the shapes of inflated diaphragms for low crown strains and the initial region ($\lambda = 1 \rightarrow 1.5$) of the force extension curve in simple extension. However, for the purpose for which this work was initiated, as comprehensive a PHS plot as possible was required, and so stress–strain equations containing enough curve-fitting parameters to give accurate regression to these data were sought.

In the work reported here, the two forms of approximation have been compared by determining the accuracy with which a particular form of stress–strain equation represents the PHS plot. The stress–strain equation resulting from each strain energy function approximation was used to perform a regression to the data obtained with a natural-rubber gum vulcanizate as shown in Figure 2. The residual deviation of the data about these regression lines is calculated so that the "goodness of fit" can be judged.

Shown in Table III are the regression constants obtained with the various approximations of W described earlier, together with the residual deviations of

TABLE III
(MN/m²)

Constant	No. of constants	C_{10}	C_{01}	C_{11}	C_{20}	C_{02}	C_{21}	C_{12}	C_{30}	C_{03}	C_{40}	Res. dev.
Type of approximation		$\times 10^{-1}$	$\times 10^{-2}$	$\times 10^{-3}$	$\times 10^{-4}$	$\times 10^{-5}$	$\times 10^{-5}$	$\times 10^{-5}$	$\times 10^{-5}$	$\times 10^{-7}$	$\times 10^{-5}$	
1st-Order Invariant "Mooney"	2	2.12	0.79									0.087
2nd-Order Invariant	5	2.00	1.15	−0.22	7.89	0.48						0.078
3rd-Order Invariant	9	2.11	2.15	−1.78	−8.25	10.5	8.23	−1.45	7.16	7.10		0.051
2nd-Order Deformation	3	2.10	0.78		0.57							0.087
3rd-Order Deformation	5	2.17	1.76	−0.64	−24.1				16.8			0.055
4th-Order Deformation	8	2.20	2.92	−2.78	−57.6	−4.67	11.7		78.4		−3.04	0.040

the data contained in Figure 2 about the regression lines. The table shows that as the order of terms included increases, the residual deviation decreases, indicating a better fit to the PHS plot. The deformation approximations are seen to be somewhat more successful than the invariant approximations, achieving better fits with equations containing fewer terms.

The stress–strain relations suggested by the coefficients in Table III have been used in a number of model design experiments. All of these relations were found to be suitable for the prediction of experimental results, although the higher order equations gave greater accuracy and in some cases better extrapolation outside the range of experimental strains encompassed by the PHS plot. Some typical experimental predictions are described in the next section and illustrated using the most successful stress–strain forms.

THE APPLICATION OF STRESS–STRAIN RELATIONS TO DESIGN CALCULATIONS

Experiments in Simple Tension

Consider the condition for simple extension of a strip of rubber substituted into eq. (4), namely,

$$\sigma_1 = F_1\lambda_1 \quad \sigma_2 = 0 \qquad \lambda_2 = 1/\sqrt{\lambda_1}$$

$$F_1\lambda_1 = (\lambda_1^2 - 1/\lambda_1)\left|\frac{\partial W}{\partial I_1} + 1/\lambda_1 \frac{\partial W}{\partial I_2}\right|$$

or

$$F = (\lambda_1 - \lambda_1^{-2})\left|\frac{\partial W}{\partial I_1} + 1/\lambda_1 \frac{\partial W}{\partial I_2}\right|$$

where F is the stress referred to the original cross-sectional area. Using this equation and some form of the strain energy function, it is a simple matter to compute a simple extension stress–extension ratio curve. A number of these were computed and compared to experimental results obtained by extending a strip of natural-rubber gum in an Instron tensile tester.

The experiment was performed incrementally allowing 5 mins relaxation at each increment. It was assumed that this gave the same sort of quasi equilibrium data obtained in the general homogeneous strain experiment described earlier.

Figure 4 shows the comparison between simple extension experimental results to $\lambda = 5.0$ and results predicted from the stress–strain relations calculated from the coefficients of Table I. These describe the PHS plot where extension ratios are less than 3.5. The relations with a lower residual deviation about the PHS plot gave a more accurate prediction of the experimental results. The best predictions are shown in the figure. The third- and fourth-order deformation approximations and the third-order invariant approximation accurately predicted the experimental result within the range encompassed by the PHS plot ($\lambda < 3.5$). However, the third-order invariant approximation also extrapolated well outside this range. The odd behavior of the fourth-order approximation outside the experimental range is not necessarily significant. One must not lose sight of the fact that the equations are merely regression equations. To fit

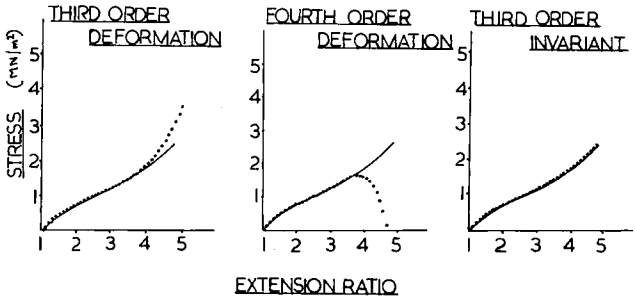

Fig. 4. Stress vs. extension ratio for NR gum: (· · ·) theory; (——) experiment. Abscissa: extension ratio λ_2; ordinate stress $\sigma_i - \sigma_j$(NM/m²).

more accurately in regions where data are available, terms in the equation can take signs which may result in apparent unusual behavior in regions where no data are available.

Experiments in Equibiaxial Extension

If an element at the crown of an inflated membrane is considered, the tensions in the latitudinal and longitudinal directions being T_1 and T_2 and the respective radii of curvature R_1 and R_2, then these quantities are related to the inflation pressure P according to the equation

$$P = T_1/R_1 + T_2/R_2$$

at the crown

$$T_1 = T_2 = T$$

$$R_1 = R_2 = R$$

$$\therefore \quad P = 2T/R.$$

If the thickness of the strained material is t then the stress at the crown is given by

$$T/t = \sigma$$

$$\therefore \quad \sigma = PR/2t \cdots \tag{6}$$

and for an incompressible material stretched equibiaxially by λ, the third dimension is reduced by $1/\lambda^2$; thus $t = t_0/\lambda^2$, where t_0 is the original thickness. Thus, the crown stress can be found for a particular crown strain providing P, R, and t_0 can be measured.

A diaphragm was inflated to a particular pressure and the crown-extension ratio λ_c was calculated from measurements of the vertical and horizontal distances between points on a grid.

The radii of curvature were then calculated geometrically and the stress at a particular extension calculated from eq. (6). A graph of the equibiaxial stress versus-extension ratio is shown in Figure 5 for the natural rubber gum vulcanizate. The full line drawn through the experimental values was predicted using regression constants from Table I to calculate values of $\partial W/\partial I_1$ and $\partial W/\partial I_2$ in the general stress–strain equation in its equibiaxial extension form:

$$\sigma = (\lambda^2 - \lambda^{-4}) \left| \frac{\partial W}{\partial I_1} + \lambda^2 \frac{\partial W}{\partial I_2} \right|.$$

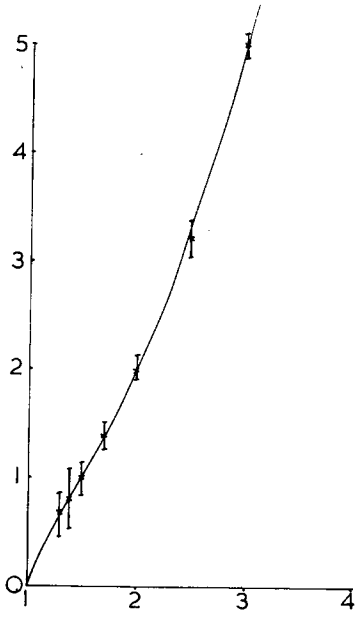

Fig. 5. Equibiaxial extension: (——) predicted curve; (X) - - -

Again, the agreement between theory and experiment is excellent, and the line shown is the coincident predictions of the third- and fourth-order deformation approximations and the third-order invariant approximations. The lower-order approximations predicted the general shape of the curve but with a less accurate fit to the experimental values.

The Mooney-Rivlin Plot

A way of representing all the data of the above two sections is the so-called Mooney-Rivlin plot. The general stress–strain equation can be rearranged using the conditions for simple extension to the form

$$F/2\left|\lambda - \lambda^{-2}\right| = \frac{\partial W}{\partial I_1} + 1/\lambda \cdot \frac{\partial W}{\partial I_2} \cdots \tag{7}$$

also the same equation can be rearranged in the same way by substituting the conditions for equibiaxial extension, viz.,

$$\sigma_1 = F\lambda_1 \quad \lambda_1 = \lambda, \qquad \lambda_2 = \lambda_3$$

to give

$$F/2\left|\lambda - \lambda^{-2}\right| = \partial W/\partial I_1 + 1/\lambda \cdot \partial W/\partial I_2 \cdots \tag{8}$$

Equations (7) and (8) are identical, and so a graph of $F/2\left|\lambda - \lambda^{-2}\right|$ versus $1/\lambda$ can be made to include information from the measurements of both the above sections.

Figure 6 is typical of such a plot and contains the same information as that contained in Figures 4 and 5. These plots have probably become accepted as a good criterion of a stress–strain equation because they show information from both simple tension and equibiaxial extension and have certain distinctive fea-

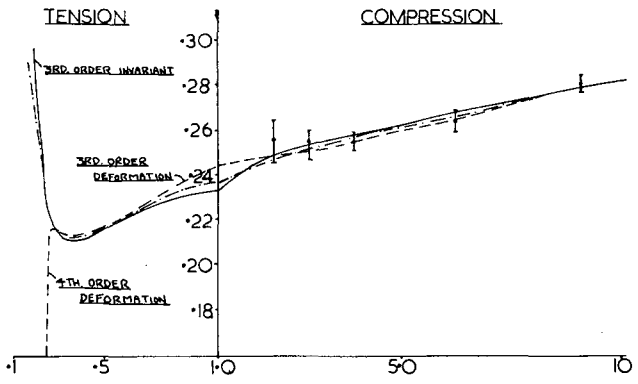

Fig. 6. The Mooney-Rivlin plot. Abscissa: $1/\lambda$ (note change of scale at $\lambda = 1.0$); ordinate: $F/2(\lambda^{-1} - \lambda^{2})$.

tures, namely, the linear region at low simple extensions, the upturn at high simple extensions, and the plateau region in equibiaxial extensions. However, experimental data obtained as in the previous sections seem to indicate a discontinuity at $1/\lambda = 1$. This has recently been shown not to be true by Wolfe,[16] who demonstrated the continuity of the relationship in going from simple extension into uniaxial compression. Also, by the methods described above, it is difficult to get accurate information in the region $1/\lambda \rightarrow 1$.

The first-order invariant approximation, the so-called Mooney equation cannot predict all the features of this plot, and the two second-order approximations resulted in equations which showed large discrepancies when fitted to the experimental data in this way. However, as can be seen from Figure 6, the approximations which were successful in the previous sections also reproduce the main features of this plot, the notable exception again being the failure of the fourth-order deformation approximation to predict high simple extensions. However, within the range of strains encompassed by the PHS plot, these three approximations showed reasonable accuracy.

The Inflated Membrane

Equations (4) and the procedure described earlier for finding the material constants give stress–strain relations which have been shown to be successful in describing certain experimental deformations. As a more practical test typical of engineering design, it was decided to use this equation to predict the total profile of an inflated membrane which will necessarily involve a more general biaxial deformation. Appendix I gives a description of the numerical solution of the shape of an inflated diaphragm.

In the approach used successfully by Hart-Smith,[11] the solution involved the use of first-order numerical integration as opposed to the more straightforward method of "approximating arcs."

The method described in Appendix I incorporates techniques of both approaches; and given the regression coefficients and the crown extension λ_c, we may predict the inflation pressure P and the shape of an inflated diaphragm.

A computer program was written to carry out the procedure described in Appendix I containing a subroutine to plot out directly the profile relevant to a particular set of material constants.

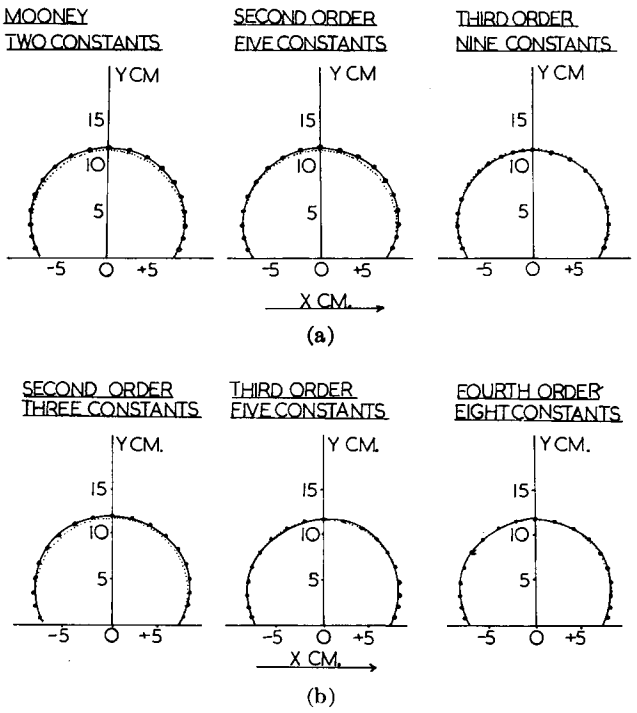

Fig. 7. (a) NR gum diaphragm profiles calculated from invariant approximations—crown strain $\lambda_c = 3.0$: (—O—) theory; (. . . .) experiment. Abscissa: $1/\lambda$ (note change of scale at $\lambda = 1.0$); ordinate: $F/2(\lambda^{-1}/\lambda^2)$. (b) NR gum diaphragm profiles calculated from deformation approximations—crown strain $\lambda_c = 3.0$: (—O—) theory; (. . . .) experiment. Abscissa: $1/\lambda$ (note change of scale at $\lambda = 1.0$); ordinate: $F/2(\lambda^{-1}/\lambda^2)$.

Equation (4) and the Table II coefficients were used to predict diaphragm profiles for a range of crown extensions up to $\lambda_c = 4.0$. These were compared with experimental profiles (obtained on the apparatus described above). In Figures 7A and B, profiles for $\lambda_c = 3.0$ calculated using the different approximations of the strain energy function are compared with experiment. Again, the higher-order approximations are seen to be more accurate, although the difference is not so great at low extensions. Up to the maximum strains of the PHS plot which are greater than those experienced in most engineering practice, the higher-order approximations of the strain energy function give stress–strain equations accurate enough for most practical purposes. There is also good agreement between the predicted and experimentally measured inflation pressures.

The Inflated Tube

Another problem which can be solved by techniques similar to those described in the previous section is the longitudinal cross-sectional profile of an inflated tube, the ends of which are free to find their own position. Appendix II gives a description of the numerical solution of the shape of an inflated tube.

The inflated tube apparatus consists essentially of two circular clamps, which hold a rubber tube onto mandrils attached to the load cell and cross head of an Instron tensile tester. One of the circular mandrils was such that air could be blown through it into the tube. The tubular sample was moulded to give the

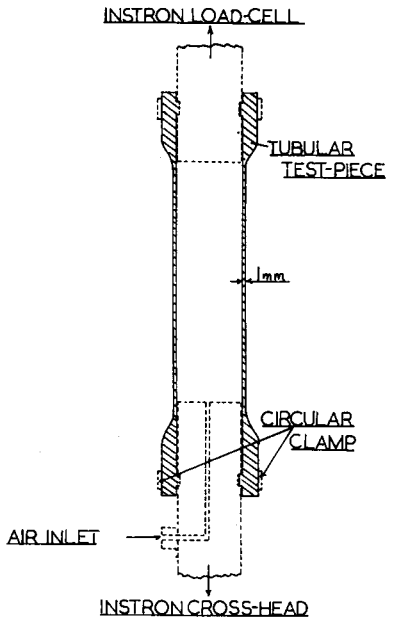

Fig. 8. Cross section of tube inflation apparatus. Abscissa: $1/\lambda$ (note change of scale at $\lambda = 1.0$; ordinate $F/2(\lambda^{-1}\lambda^2)$.

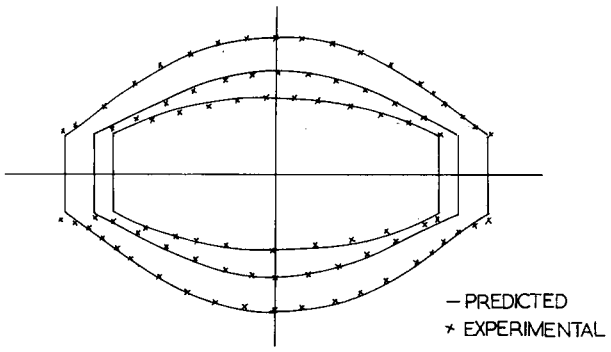

Fig. 9. Profiles of inflated tubes–NR gum.

cross section shown in Figure 8. The circumferential bars on the internal diameter at each end were located in grooves in the mandrils to give a positive grip. The tube was 1 mm thick along the length to be stretched and much thicker at each end. This gave an effective length for this extending portion of 11.5 cm.

The air pressure was measured with a pressure gauge and was controlled by a constant-pressure reducing valve. The experiments were performed so that the ends of the tube were always at zero load. As the tube was inflated, this tended to push the jaws apart, so creating a "compressive" force and giving a negative load reading. The tube was then extended so that the load, as registered by the Instron load cell, was zero. The pressures were controlled to give a range of radial extensions for the tube.

A grid on the surface of the tubular sample facilitated strain measurements. The inflated tubes were photographed and the negatives examined using an

inspection microscope. Using eqs. (4) and the material constants of Table I, theoretical profiles were plotted and compared with profiles obtained by the above method.

Figure 9 shows three such predictions for the natural-rubber gum vulcanizate, obtained using the third-order invariant approximation. The three diagrams represent profiles obtained at three different circumferential extension ratios $\lambda_c = 1.99$, 2.68, and 3.54. There is good agreement between experiment and theory not only in the shape of the profile, but also in the final length of the inflated tube. The third-order and fourth-order deformation approximations give comparable accuracy, but the lower-order approximations result in some deviation from experimental values.

CONCLUSIONS

The foregoing results have shown that a good fit to general homogeneous strain data can be obtained by retaining higher-order terms in the expansion of the strain energy function. An expansion as far as the third order of invariants leads to stress–strain equations which can be used for the accurate solution of engineering design problems even at strains outside the range encompassed by the PHS plot from which the nine coefficients in the equation were obtained. However, for most practical purposes, the expansion as far as the third order of deformation should be adequate. This contains the five terms C_{10}, C_{01}, C_{11}, C_{20}, and C_{30}. These techniques can also be applied to filled vulcanizates, as will be described in part II of this series.

Appendix I

The Numerical Solution of the Shape of an Inflated Diaphragm

Notation. The notation used in the theory that follows is presented below. Also, as an aid to the understanding of the "approximating arc" technique, an illustrative diagram (Fig. 10) is included.

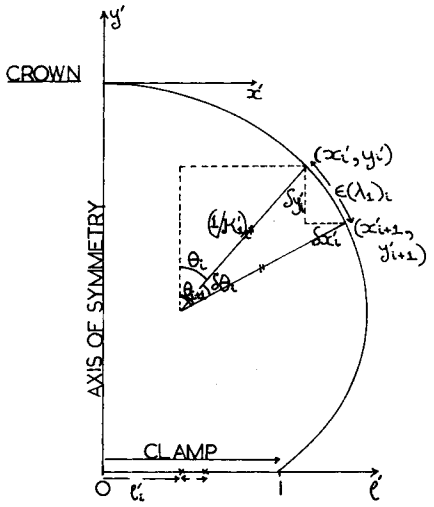

Fig. 10. Half a meridional section scaled to clamp radius = 1.

N.B.: (1) Dashed symbols represent variables that have been nondimensionalized. (2) Symbols with suffixes, e.g., x_i', $(T_1')_t$, $(\lambda_1)_t$, etc., represent the values of the variables at particular points chosen on the sheet.

W strain energy function
G factor to nondimensionalize $W(=C_{10})$
P inflation pressure
T_1 meridional tension
T_2 circumferal tension
κ_1 meridional curvature
κ_2 circumferal curvature
λ_1 meridional extension ratio
λ_2 circumferal extension ratio
I_1, I_2 } strain invariants
λ_c extension ratio under equibiaxial conditions at the crown
ρ radial displacement from the center of the uninflated sheet
ρ_t radius of the clamp
x horizontal displacement from the crown of the inflated shape
y vertical displacement from the crown of the inflated shape
θ angular displacement measured from the y-axis

Theory

The basic equations used in this method are the stress/strain equations,

$$T_1 = 2h \cdot \lambda_3|\lambda_1^2 - \lambda_3^2||\partial W/\partial I_1 + \lambda_2^2\, \partial W/\partial I_2|\cdots \tag{1}$$

$$T_2 = 2h \cdot \lambda_3|\lambda_2^2 - \lambda_3^2||\partial W/\partial I_1 + \lambda_1^2\, \partial W/\partial I_2|\cdots \tag{2}$$

and the equilibrium conditions,

$$\kappa_1 T_1 + \kappa_2 T_2 = \mathrm{P}\cdots \tag{3}$$

$$2\kappa_2 T_1 = \mathrm{P}\cdots \tag{4}$$

where eq. (3) is from considerations of an element of double curvature and eq. (4) from considerations of a cap symmetrical about the y-axis.

As in 11, we first nondimensionalize quantities where possible, i.e., (i) Divide linear dimensions x, y, ρ, R_1, R_2, by ρ_t, the radius of the clamp (where $R_1 = 1/\kappa_1$ and $R_2 = 1/\kappa_2$ are radii of curvature), e.g.,

$$x' = x/\rho_t$$

$$\kappa_1' = \kappa_1 \rho_t$$

and

$$\rho_t' = 1.$$

N.B.: The quantities $\lambda_2, \lambda_2, \lambda_3$ will remain unchanged.
(ii) Divide W by G, T_1 and T_2 by $2hG$, and P by $2hG/\rho_t$. Thus,

$$W' = W/G$$

$$T_i' = T_i/2hG \qquad i = 1, 2$$

$$P' = P\rho_t/2hG.$$

Therefore, eqs. (1) to (4) become

$$T_1' = \lambda_3|\lambda_1^2 - \lambda_3^2||\partial W'/\partial I_1 + \lambda_2^2\, \partial W'/\partial I_2|\cdots \tag{1a}$$

$$T_2' = \lambda_3|\lambda_2^2 - \lambda_3^2||\partial W'/\partial I_1 + \lambda_1^2\, \partial W'/\partial I_2|\cdots \tag{2a}$$

$$\kappa_1' T_1' - \kappa_2' T_2' = P'\cdots \tag{3a}$$

$$2\kappa_2' T_1' = P'\cdots \tag{4a}$$

Also, if we eliminate P' between (3a) and (4a) and rearrange, we have

$$\kappa_1' = \kappa_2'(2 - T_2'/T_1')\cdots \tag{5a}$$

The problem now is to find the inflated shape and the nondimensionalized inflation pressure P' of a diaphragm of unit radius such that the extension ratio at its crown is λ_c. To do this, we proceed as follows:

(i) The unit radius of the uninflated diaphragm is divided into n equal parts such that the length of each is $\epsilon = 1/n$. It is assumed that each of these in a meridional section through the inflated shape may be considered to approximate to an arc of a circle, curvature $(\kappa_1)_i$, where $i = 1$ for the crown and $i = (n + 1)$ for the point at which the material is clamped.

(ii) The calculation of the shape is initiated at the crown where we have the equibiaxial conditions

$$(\lambda_1)_1 = (\lambda_2)_1 = \lambda_c,\ (\lambda_3)_1 = 1/\lambda_c^2$$

$$(T_1')_1 = (T_2')_1 = T_c'$$

$$(\kappa_1')_1 = (\kappa_2')_1 = \kappa_c'.$$

However, the curvature at the crown is not known and so to proceed, we must assume a value for κ_c' which may be corrected at a later stage.

Hart-Smith and Crisp[11] suggest an approximation to κ_c' based on the solution of the problem of a diaphragm of nonuniform thickness that on inflation takes the shape of a spherical cap, i.e.,

$$\kappa_c' = 2\sqrt{\lambda_c - 1/\lambda_c}.$$

Now using either (1a) or (2a), we may calculate T_c' and hence find a first approximation of P'. Thus, from (4a),

$$P' = 2\kappa_c' T_c'.$$

Also, since the height of the inflated shape is initially unknown, it is convenient to use the crown as the origin of the x', y' coordinate frame, thus,

$$\rho_1' = 0$$

$$x_1' = 0$$

$$y_1' = 0$$

$$\theta_1 = 0.$$

When the calculation is complete, the inflated shape may be defined with respect to the center of the uninflated diaphragm by subtracting y'_{n+1} from all values y_i', $i = 1, 2\ldots, (n + 1)$.

(iii) To calculate the x', y' coordinates of the next and subsequent point, the following procedure is applied. We have the geometric relationships (see Fig. 10) for $i = 1, 2\ldots, (n - 1), n$

$$\rho_{i+1}' = \rho_i' + \epsilon$$

$$\theta_{i+1} = \theta_i + \delta\theta_i$$

where $\delta\theta_i = (\lambda_1 \epsilon \kappa_1')_i$ from the "approximating arc" assumption

$$x_{i+1}' = x_i' + \delta x_i'$$

$$y_{i+1}' = y_i' + \delta y_i'$$

where

$$\delta x_i = (\sin(\theta_{i+1}) - \sin(\theta_i))/(\kappa_1')_i$$

and

$$\delta y_i = (\cos(\theta_{i+1}) - \cos(\theta_i))/(\kappa_1')_i$$

$$(\kappa_2')_{i+1} = \sin(\theta_{i+1})/x_{i+1}'$$

$$(\lambda_2)_{i+1} = (x'/\rho')_{i+1}.$$

However, to find $(\lambda_1)_{i+1}$, we must use an iterative procedure starting with an approximation λ^*_1 for λ_1 (see note on approximations). From (4a), we see that

$$T_1' = P'/2\kappa_2'.$$

Now, (1a) may be rearranged to form an iterative procedure, thus,

$$\lambda^*_1 = 1/(\lambda_2\lambda^*_1)$$

$$\lambda_1 \simeq \lambda^{*}_3{}^2 + \frac{T_1'}{\lambda^*_3|\partial W'/\partial I_1 + \lambda_2{}^2\ \partial W'/\partial I_2|} \tag{6}$$

where

$$I^*_1 = \lambda^*_1{}^2 + \lambda_2{}^2 + \lambda^*_3{}^2$$

and

$$I^*_2 = \lambda^*_1{}^{-2} + \lambda_2{}^{-2} + \lambda^*_3{}^{-2}.$$

The l.h.s. of (6) will yield a new approximation to λ_1, and the iterative process may be repeated until successive approximations agree to within defined limits (e.g., $10^{-4}\lambda_1$).

Having found the value of $(\lambda_1)_{i+1}$, we may evaluate $(T_2')_{i+1}$ and $(\kappa_1')_{i+1}$ using eqs. (2a) and (5a), respectively.

At this stage, we know all the quantities at the $(i + 1)$th point, and the process may be repeated to find the coordinates of the next and subsequent points, until either

$$\text{(i) } \lambda_2 \leq 1 \text{ and } i < (n)$$

or

$$\text{(ii) } i = (n) \text{ and } \lambda_2 \neq 1$$

If one of these conditions is satisfied, we find the value of x', say, x'_{FAC}, which makes $\lambda_2 = 1$, using linear interpolation and use this to correct the original estimate of κ_c', thus,

$$(\kappa_c')_{\text{NEW}} = (\kappa_c')_{\text{OLD}} \cdot x'_{\text{FAC}}.$$

The calculation is then repeated from the crown using the new κ_c' until x_n' differs from unity only by narrow defined limits (e.g., $\pm 10^{-4}$).

Note: On the choice of the original approximation to λ_1, it has been found that a good approximation (requiring two to three iterations to reach "true solution") is given by

$$(\lambda^*_1)_{j+1} = (\lambda_1)_{j-2} + 3|(\lambda_1)_j - (\lambda_1)_{j-1}|.$$

This is, in fact, equivalent to fitting a parabola through the three points $i = j - 2$, $j - 1$, and j on a (λ_1, ρ) plot and extrapolating to $i = j + 1$.

Further, it has been found[11] that to ensure the convergence of the iterative procedure for $\lambda_c > 5$, it is necessary to average successive approximations.

A computer program has been written to perform the solution method described and to draw the inflated shape on a digital plotter.

Appendix II

The Numerical Solution of the Shape of an Inflated Tube

INTRODUCTION

A method of solution to the problem of an inflated tube has been evolved using a similar approach to that applied to the inflated diaphragm. The problem is to find the longitudinal shape and the necessary inflation pressure (P) of a tube of given unstrained length ($2l_0$) and radius (r_0), such that the radius (r_w) at the widest point (w) on the shape is a given constant and the radii at the ends are equal to the strained radius.

This problem differs from that of the diaphragm in that, for the latter, (i) there is a condition of equibiaxial stress at pole, i.e.,

$$\lambda_1 = \lambda_2 = \lambda_c$$

(ii) an adequate approximation to the curvatures

$$(\kappa_1 = \kappa_2 = \kappa_c)$$

at the pole is available; (iii) successively better approximations to the solution are obtained by simple scaling at the end of each contour calculation.

Whereas for the tube (i) only one of the principal extensions

$$(\lambda_2 = \lambda_w = r_w/r_0)$$

at the starting point (w) of the calculation is known, λ_1 being unknown; (ii) no approximation to one of the principal curvatures (κ_1) at W is available, although the other, κ_2, is given directly by

$$\kappa_2 \text{ at } w = 1/r_w.$$

(iii) Simple scaling cannot be used to obtain better approximations to the true solution.

Thus, to solve the tube problem the following approach was taken: (i) Assume that the unstrained length, $2l_0$, of tube is allowed to vary, all other dimensions remaining fixed (i.e., radius, thickness); (ii) choose some approximation λ_a to λ_1 at w and calculate the corresponding shape subject to the conditions at the widest and end points. It should be noticed that the unstrained length, $2l_a$, corresponding to this inflated shape will not be the same as $2l_0$ unless λ_a is a very good estimate; (iii) use interpolation/extrapolation and other techniques, on a (λ_a, $1/l_a$) plot, to correct λ_a to give an unstrained length of $2l_0$.

THEORY

The Inflated Shape Calculation

The equation and notation used in the following theory are similar to those for the diaphragm. For further explanation, reference may be made to Appendix I and to Figure 11 of this paper.

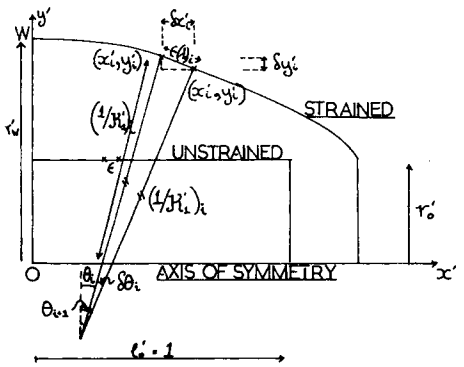

Fig. 11. Tube: $^1/_4$ of a plane section through the axis of symmetry. Scaled to $^1/_2$ tube length = 1.

The stress/strain equations are

$$T_1 = 2h\lambda_3|\lambda_1^2 - \lambda_3^2||\partial W/\partial I_1 + \lambda_2^2\,\partial W/\partial I_2| \tag{1}$$

$$T_2 = 2h\lambda_3|\lambda_2^2 - \lambda_3^2||\partial W/\partial I_1 + \lambda_1^2\,\partial W/\partial I_2| \tag{2}$$

The equilibrium conditions are

$$\kappa_1 T_1 + \kappa_2 T_2 = P \tag{3}$$

$$2\kappa_2 T_1 = P. \tag{4}$$

As in the previous Appendix, we nondimensionalize quantities, in this case using half the tube length (i.e., l_0) instead of the clamp radius as the linear factor, e.g.,

$$r_0' = r_0/l_0$$

$$l_0' = 1$$

$$x' = x/l_0$$

$$\kappa_1' = \kappa_1 l_0$$

$$T_1' = T_1/2hG$$

$$P' = Pl_0/2hG$$

$$W' = W/G$$

Thus, nondimensionalizing and eliminating P from (3) using (4), we have, from eqs. (1)–(4),

$$T_1' = \lambda_3|\lambda_1^2 - \lambda_3^2||\partial W'/\partial I_1 + \lambda_2^2\,\partial W'/\partial I_2| \tag{1a}$$

$$T_2' = \lambda_3|\lambda_2^2 - \lambda_3^2||\partial W'/\partial I_1 + \lambda_1^2\,\partial W'/\partial I_2| \tag{2a}$$

$$P' = 2\kappa_2' T_1' \tag{3a}$$

$$\kappa_1' = \kappa_2'(2 - T_2'/T_1'). \tag{4a}$$

Also, we have the geometric relationships

$$\delta\theta_i = \epsilon(\lambda_1)_i(\kappa_1')_i$$

where

$$\epsilon = 1/(n-1) \text{ (the step size)}$$

$$\theta_{i+1} = \theta_i + \delta\theta_i$$

$$\delta x_1 = |\sin(\theta_{i+1}) - \sin(\theta_i)|/(\kappa_1')_i$$

$$\delta y_i = |\cos(\theta_{i+1}) - \cos(\theta_i)|/(\kappa_1')_i$$

$$x_{i+1} = x_i + \delta x_i$$

$$y_{i+1} = y_i + \delta y_i$$

$$(\kappa_2')_{i+1} = \cos(\theta_{i+1})/y_{i+1}'$$

$$(\lambda_2)_{i+1} = y_{i+1}'/r_0'.$$

These equations may be solved using the techniques applied to the diaphragm solution, where for some approximation λ_a, to λ_1 at w, the corresponding l_a' is given by

$$l_a' = \epsilon(N - m)$$

where N is the number of whole increments required during the computation to reach the region of the end clamp ($\lambda_2 \simeq 1$) and m is the fractional part of an increment required to fit the end point to the unstrained radius ($\lambda_2 = 1$).

Convergence to the "true" Solution

We see that, from the section above, given any approximation λ_a to λ_1 at w, we may calculate an inflated shape (given λ_w and r_0), an inflation pressure, and the corresponding unstrained length of the tube. The following section deals with a method of correcting λ_a to ensure convergence to the solution $l_a' = l_0' = 1$.

(i) The first stage of ensuring convergence is to limit the range in which λ_a may vary. It has been found that, for the tubes used experimentally, the configuration (i.e., $l_0/r_0 \simeq 3.5$) is such that the "true" λ_1 is always significantly less than λ_2 at w (i.e., $\kappa_1 < \kappa_2$ at w). Further, we see that at w, $\kappa_1 > 0$ (i.e., w is a point of maximum width); thus, from (4a) we see that for $\kappa_1 = 0$:

$$2T_1' - T_2' = 0 \tag{5}$$

where T_1' and T_2' are given in terms of λ_1, λ_2, and the material constants. Now, eq. (5) may be solved by simple techniques, for $\lambda_2 = \lambda_w$ and given material constants, to give the solution $\lambda_1 = \lambda_z$, say. Thus, λ_a is restricted to vary in the range (λ_z, λ_w).

(ii) However, for certain values of λ_w (usually >2), it has been found, for values of λ_a in the range, say, (λ_z, λ_t) where $\lambda_z < \lambda_t < \lambda_w$, that the contour shape when computed tends to oscillate, never satisfying the condition on the endpoint (i.e., is always greater than unity). In this case, the computation is ended at the point at which λ_2 is a minimum (i.e., when θ is again zero) and the unstrained length to this point calculated and the information obtained is used to tighten the range in which λ_a may vary. Notice that λ_z may be considered to be an extreme of this case giving zero unstrained length.

(iii) For $\lambda_t < \lambda_a < \lambda_w$, we are able to compute shapes and values of l_a' that satisfy the endpoint conditions; and when four sets of λ_a, $1/l_a'$ data, in this range, are available, a cubic curve can be fitted and a very close approximation to the "true" solution found. The cubic fitting may be repeated, if necessary, with the latest set of data replacing that most removed from the "true" solution, until the computed l'_a agrees with unity to within close limits.

The first approximation to λ_1 at w is taken to be λ_w and the corresponding l_a' calculated. Using linear interpolation, shown schematically in Figure 12, a second estimate may be found and, if necessary, the range in which λ_a may vary tightened. This is repeated until the four sets of data for the cubic fit are obtained.

A computer program has been written to perform the solution as described and to draw the calculated inflated shapes on a digital plotter.

An alternative method of solving this problem is given by Kydoniefs[18] where the inflated shape is found by numerical integration rather by the "approximating arcs" method given here. However, the numerical integration becomes lengthy with more complicated strain energy functions.

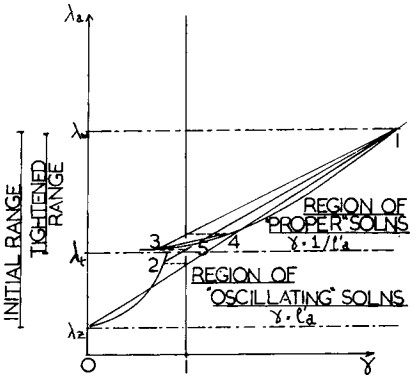

Fig. 12. Length approximation: (1) initially $\lambda_a = \lambda_w$; (2) used to tighten range; (3) further approximations in the (4) "proper" solution regions; used (5) with 1 for the cubic fit.

The authors wish to thank P. S. Oubridge and G. D. Hubbard for helpful criticism and discussion, and the Dunlop Co. for permission to publish this paper.

References

1. R. S. Rivlin and D. W. Saunders, *Phil. Trans. Roy. Soc.*, **865**, 243 (1951).
2. L. R. G. Treloar, *Physics of Rubber Elasticity*, Clarendon Press, 1949.
3. A. E. Green and W. Zerna, *Theoretical Elasticity*, Oxford Univ. Press, 1954.
4. L. R. G. Treloar, *Proc. Phys. Soc.*, **60**, 135 (1948).
5. K. Sakaguchi, S. Kawabata, N. Hasama, and H. Kawai, *Zairyo*, **17**, 356 (1968).
6. Y. Obata, S. Kawabata, and H. Kawai, *J. Poly. Sci.*, **8**, 903 (1970).
7. M. Mooney, *J. Appl. Phys.*, **18**, 444 (1947).
8. A. Isahara, N. Hashitsume, and M. Tatibaua, *J. Chem. Phys.*, **19**, 1508 (1951).
9. A. N. Gent and A. G. Thomas, *J. Poly. Sci.*, **28**, 118 (1958).
10. W. W. Klingbeil and R. T. Shield, *Z. Angew Math. Phys.*, **15**, 698 (1964).
11. L. J. Hart-Smith, *Z. Angew Math. Phys.*, **17**, 608 (1966).
12. K. C. Valanis and R. F. Landel, *J. Appl. Phys.*, **38**, 7 (1967).
13. R. W. Ogden, *Proc. R. Soc.*, **A326**, 565 (1972).
14. N. W. Tschoegl, *J. Poly. Sci.*, **9**, 1959 (1971).
15. V. L. Bidemann, *Raschetti na Prochnost*, 15.5 18.1 (1958).
16. Y. Sato, *Reports on Progress in Poly. Phys. in Japan*, **XVI** (1973).
17. F. P. Wolf, *Polym.*, **13**, 347 (1972).
18. F. Kydoniefs, *Quat. J. Mech. and Appl. Math.*, **22**, (1969).

Received September 10, 1974
Revised December 23, 1974